Research Square

Preprints are preliminary reports that have not undergone peer review.
They should not be considered conclusive, used to inform clinical practice,
or referenced by the media as validated information.

Field application of sand-ceramsite in-filled pile barrier in mitigating metro train-induced vibrations

Weili Luo

wlluo@gzhu.edu.cn

Guangzhou University

Shibang Deng

The Hong Kong Polytechnic University

Research Article

Keywords: metro train-induced vibrations, mitigation countermeasure, sand-ceramsite mixture, field application, wave barrier

Posted Date: November 10th, 2026

DOI: https://doi.org/10.21203/rs.3.rs-11065152/v1

License: This work is licensed under a Creative Commons Attribution 4.0 International License.
Read Full License

Additional Declarations: No competing interests reported.

Field application of sand-ceramsite in-filled pile barrier in mitigating metro train-induced vibrations

Abstract. Vibrations generated by metro train operations can propagate to nearby structures and cause discomfort to residents. To mitigate this problem, this study proposes a sand-ceramsite in-filled pile barrier (SCIPB), which consists of a row of piles filled with a sand-ceramsite mixture and installed along the vibration propagation path. Details of the field application of the SCIPB are presented, and a series of in-situ tests are conducted to evaluate its vibration mitigation performance. The test results show that the SCIPB can reduce ground vibrations by up to 63%, with a maximum average insertion loss of 14.6 dB. A finite element model is then developed and validated against the field measurements. Subsequently, a numerical parametric study is performed to investigate the effects of key pile-barrier parameters. The results indicate that the vibration mitigation performance of the SCIPB can generally be improved by (a) increasing the number of pile rows, (b) decreasing the pile spacing, and (c) using in-fill materials with a lower Young's modulus.

Keywords: metro train-induced vibrations; mitigation countermeasure; sand-ceramsite mixture; field application; wave barrier

1. Introduction

In recent years, China's metro network has expanded rapidly in response to economic development. Although metro systems provide convenient and efficient transportation for millions of commuters, vibration and noise pollution have become increasingly important concerns. When buildings are constructed near existing metro tunnels, metro train-induced vibrations can propagate through the surrounding soil and reach nearby structures. These vibrations, along with the associated structure-borne noise, may cause discomfort to residents, interfere with sensitive medical equipment and laboratory instruments, and potentially affect structural safety (Bhattacharjee et al. 2025; Ni et al. 2025; Zou et al. 2025).

Measures for mitigating metro train-induced vibrations can be applied at three stages: the source, the propagation path, and the receiving structure. Source-side measures, such as rail fasteners (Alsharo et al. 2024; Gao et al. 2023), ladder sleeper tracks (Pu et al. 2025), and floating slab tracks (Ren et al. 2023; Dai et al. 2025), are generally the most effective because they directly reduce vibration generation within the tunnel. Receiver-side measures, including room-in-room systems (Fiala et al. 2007), tuned mass dampers (Liu et al. 2026), and base isolation systems (Luo et al. 2024; Luo and Deng 2026b), can also provide reliable protection for buildings exposed to transmitted vibrations. However, when source-side or receiver-side measures are not feasible, propagation-path measures offer a practical alternative because they avoid costly modifications to existing tunnels or buildings. These measures usually involve installing wave barriers along the propagation path to alter the vibration transmission characteristics of the medium. Common wave

barriers include wave impeding blocks (Cao et al. 2024), mass barriers (Dijckmans et al. 2015), concrete walls (Luo and Deng 2025), open trenches (Chango et al. 2025), and in-filled trenches (Luo and Deng 2026a). Although open trenches are theoretically highly effective because they can strongly reflect incident waves, their limited geotechnical stability often makes in-filled trenches a more practical option in engineering applications.

Many studies have investigated the vibration mitigation performance of in-filled trenches. Their effectiveness mainly depends on creating a substantial stiffness or impedance contrast between the in-filled material and the surrounding soil. Expanded polystyrene (EPS) geofoam, a lightweight and flexible material, has been widely used for this purpose. Jazebi et al. (2021) found that EPS geofoam-filled trenches could effectively reduce train-induced vibrations at train speeds of 40–160 km/h, with higher reduction efficiency at higher train speeds. Jauhari et al. (2026) demonstrated that dual geofoam-infilled barriers could achieve up to a 77.4% reduction in peak particle velocity. Kumar et al. (2026) achieved up to 84% screening efficiency by combining an aggregate trench with an EPS geofoam trench. More recently, composite materials have been considered for use in in-filled trenches. Chew and Leong (2019) proposed a sand-rubber mixture (SRM) barrier and experimentally achieved a 75% reduction in vibration amplitude. Based on field tests, Kavand and Khadangi (2023) reported a maximum reduction of 40% in vertical ground vibrations using an SRM barrier. Zhang et al. (2022) investigated ceramsite- and sand-filled barriers through full-scale model tests. They found that continuous ceramsite- and sand-filled barriers achieved maximum attenuation values of 9.3 dB and 3.8 dB, respectively, in the middle-frequency range of 30–80 Hz. To improve environmental sustainability, recyclable materials have also been increasingly used in in-filled trenches. Surapreddi and Ghosh (2023) reported that bamboo-filled wave barriers provided performance comparable to that of open trenches, reducing vertical vibrations by 70% and 75%, respectively. Moussa et al. (2024) evaluated trenches filled with tire-derived aggregates and found that they could provide up to 30% greater vibration reduction than open trenches. In addition, Celebi et al. (2024) demonstrated that recyclable waste materials, including wood shavings, Styrofoam, and expanded glass granules, can effectively screen vibrations induced by high-speed trains.

In practice, conventional in-filled trenches often require large-scale excavation and additional retaining or support systems, which can lead to high construction costs. A more economical alternative is to form an in-filled trench using closely spaced or interlocking piles arranged in a row. The vibration mitigation performance of such pile barriers has been investigated by many researchers. Ai and Cao (2018) used the analytical layer-element method (ALEM) and the finite element method (FEM) to study the isolation performance of a single row of piles. Shan et al. (2021) conducted a parametric analysis to optimize the design of isolation piles for mitigating high-speed train-induced vibrations and highlighted the importance of pile spacing. Wang et al. (2022) systematically examined the effects of pile spacing, pile length, and barrier width on vibration isolation efficiency and proposed an optimized configuration that reduced ground vibrations by 30–50%. Li (2024) employed a coupled boundary element-finite element (BEM-FEM) method to investigate the relationship between pile-barrier performance and soil saturation. Yang and Jia (2023) developed a three-dimensional coupled ALEM–BEM method to evaluate pile barriers and confirmed their ability to reduce high-frequency vibration components. In addition, periodic pile barriers and metastructures have recently been proposed as vibration mitigation measures (Ding et al. 2026; Xiao et al. 2026; Luo and Yin 2026; Luo et al. 2026). These systems use periodic arrangements to create band gaps that restrict the propagation of waves within specific frequency ranges.

Based on the vibration reduction potential of composite in-filled materials and pile barriers, this study develops a sand-ceramsite in-filled pile barrier (SCIPB) to protect structures from metro train-induced vibrations. The field application of the SCIPB at a test site is described in detail. A series of in-situ tests were conducted, including a multichannel analysis of surface waves (MASW) test to characterize the dynamic properties of the site soil and field measurements to evaluate the vibration mitigation performance of the SCIPB in an engineering project. A numerical model was then validated using the field test results, followed by a parametric study to investigate the effects of key pile-barrier parameters on vibration mitigation performance. The main contributions of this study are twofold. First, it develops the SCIPB as a practical vibration mitigation measure for structures near metro tunnels, and its first field application confirms its effectiveness in reducing metro train-induced vibrations. Second, it provides design guidance for the SCIPB through a parametric study focused on the number of pile rows, pile spacing, and in-filled material properties.

The remainder of this paper is organized as follows. Section 2 describes the field application of the SCIPB and the in-situ tests, including the MASW test and two phases of metro train-induced vibration measurements. The test results are also presented and discussed. Section 3 validates the numerical model by comparing its results with the in-situ test data. Section 4 investigates the effects of the number of pile rows, pile spacing, and in-filled material through a parametric analysis. Finally, Section 5 summarizes the main conclusions.

2. Field application and in-situ test

2.1 Overview of the test site

Fig. 1 shows the test site, which is located near the tunnels of Guangzhou Metro Line 5. Two 33-story residential buildings with three basement levels are planned for construction at this site. The minimum distance between the basement structures and the metro tunnels is 11.0 m. The tunnels were constructed using the slurry shield method and are lined with 0.3-m-thick precast C50 reinforced-concrete segments. Each tunnel has an outer diameter of 6.0 m, and the tunnel crown is located 16.5 m below the ground surface. The trains operating on Guangzhou Metro Line 5 are six-car L-type trains with a maximum operating speed of 90 km/h.

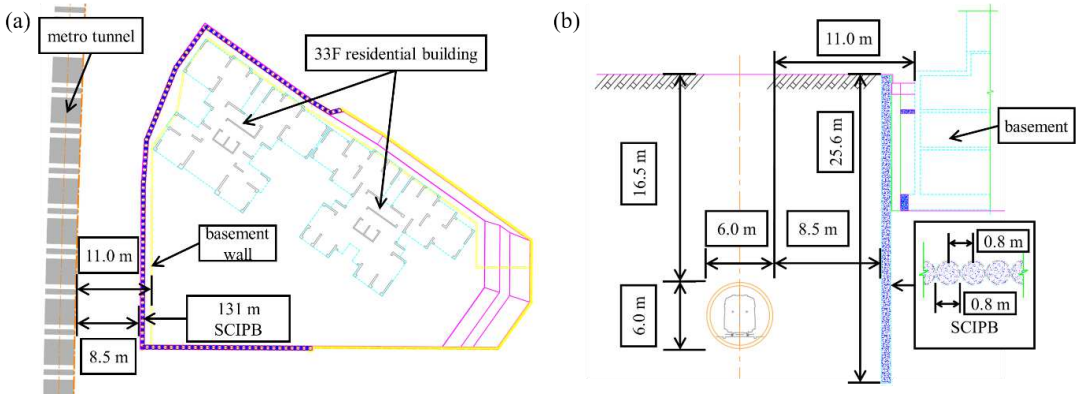


Fig. 1 Layout of the metro tunnels, planned buildings, and SCIPB: (a) plan view; (b) sectional view.

To reduce metro train-induced vibrations, a sand-ceramsite in-filled pile barrier (SCIPB) was

adopted. As shown in Fig. 2, the medium sand has particle sizes of 0.25–0.5 mm, a Young's modulus of 48.7 MPa, a Poisson's ratio of 0.30, and a dry density of 1450 kg/m³. The ceramsite is made from yellow clay and has an ellipsoidal shape. Its particle size ranges from 20 to 35 mm, and its Young's modulus, Poisson's ratio, and dry density are 5.7 MPa, 0.35, and 450 kg/m³, respectively. The sand and ceramsite were mixed at a volume ratio of 1:1 for two reasons. First, the combination provides a suitable particle-size distribution and reduces the formation of large voids. Second, the sand increases the density of the mixture, which helps ensure adequate compaction inside the pile holes by reducing the effect of buoyancy. Before field installation, the SCIPB was designed to provide effective vibration mitigation while maintaining reasonable construction costs. The barrier installed around the planned basement has a total length of 131 m and a depth of 24.5 m, extending 3.1 m below the tunnel invert. Each sand-ceramsite in-filled pile has a diameter (D) of 0.8 m.

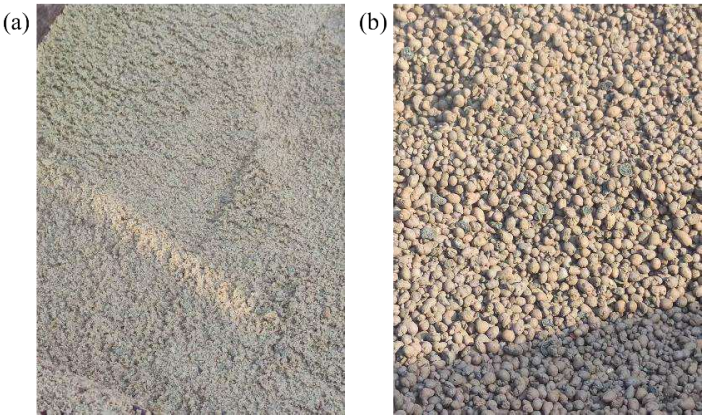


Fig. 2 Materials used in the SCIPB: (a) medium sand and (b) yellow-clay ceramsite.

2.2 MASW test

Before installing the barrier, a multichannel analysis of surface waves (MASW) test was conducted to determine the dynamic properties of the site soil. Fig. 3 shows the test setup. A hammer (Model 728A200, KSI Instruments), with a sensitivity of 25 mV/kN, was used as the excitation source. An aluminum plate was placed on the ground surface and anchored at its four corners to reduce energy loss caused by plastic deformation of the soil. Twenty-eight piezoelectric accelerometers, each with a sensitivity of 500 mV/(m/s²), were arranged in a straight line at 1-m intervals to record the vertical acceleration signals generated by the hammer impacts. The sampling frequency was set to 1000 Hz. A total of 100 hammer impacts were recorded to improve the signal-to-noise ratio.

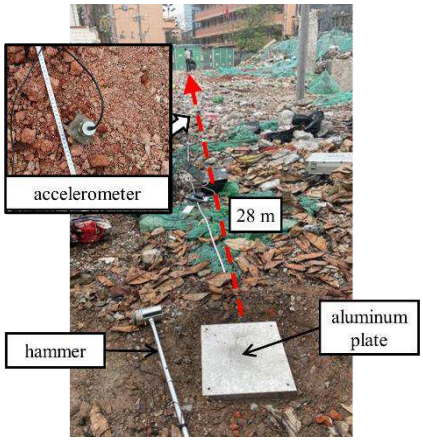


Fig. 3 MASW test setup.

Figs. 4(a) and 4(b) show the experimental and theoretical frequency-phase velocity spectra in the frequency-wavenumber domain, respectively. The theoretical fundamental-mode Rayleigh-wave dispersion curve agrees well with the experimental results at frequencies above 20 Hz. This agreement is sufficient for the simulation of metro train-induced vibrations because the dominant frequencies measured at the test site were mainly above 20 Hz, as discussed in Section 2.5. The dynamic soil properties were obtained by solving an inverse problem using the measured dispersion data. As summarized in Table 1, the upper two soil layers are underlain by a relatively stiff layer with a shear-wave velocity of 583.86 m/s.

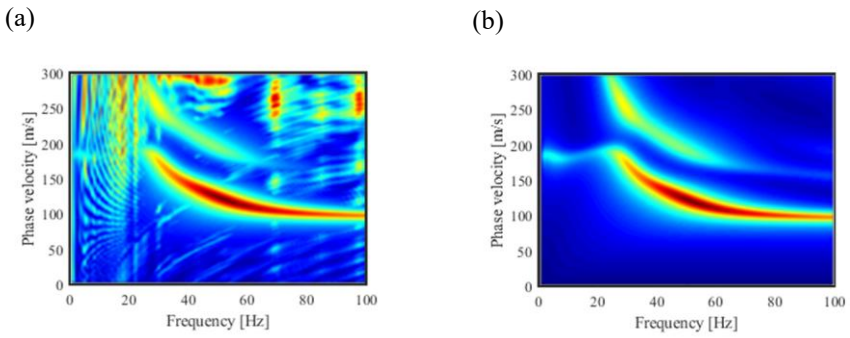


Fig. 4 Frequency-phase velocity spectra from the MASW test: (a) experimental results and (b) theoretical results.

Table 1 Dynamic properties of the soil at test site

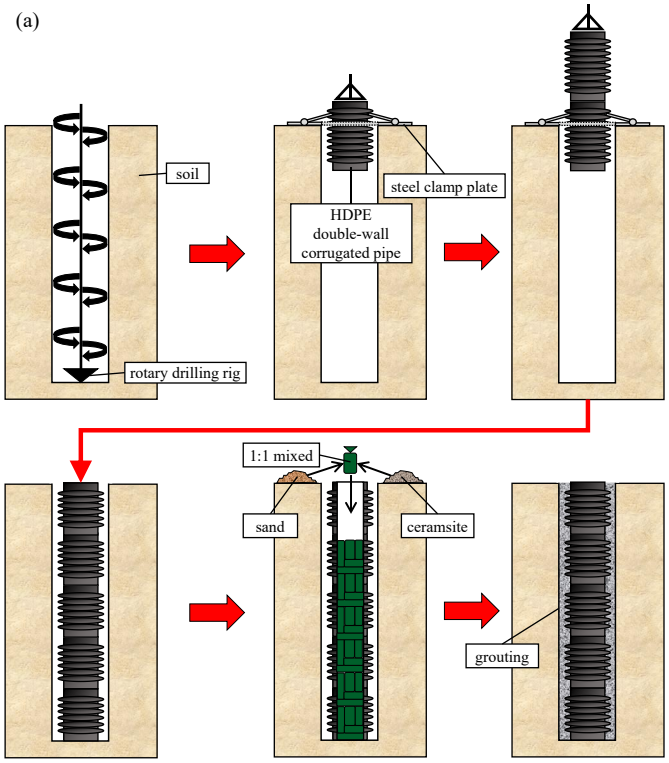
Soil layer	Thickness H (m)	Shear wave velocity C_s (m/s)	Dilatational wave velocity C_p (m/s)	Density ρ (kg/m^3)	Poisson's ratio ν (-)	Damping ratio ξ (-)
1	0.85	102.62	205.24	1800	0.33	0.05
2	2.05	178.53	357.06	1850	0.33	0.05
3	∞	583.86	1167.72	1900	0.33	0.05

2.3 Field application of the SCIPB

Fig. 5(a) illustrates the installation procedure for the sand-ceramsite in-filled piles. High-density polyethylene (HDPE) double-wall corrugated pipes were used to maintain the stability of the pile structure. The main construction steps included pile-hole drilling, installation of the multi-segment HDPE pipes, backfilling with the sand-ceramsite mixture, and grouting.

As shown in Fig. 5(b), a rotary drilling rig was used to excavate a pile hole with a diameter of 0.8 m and a depth of 25.6 m. The HDPE pipe was then lifted and lowered into the hole. Fig. 5(c) shows the connection between two adjacent pipe segments. The lower pipe segment was secured using a steel clamp plate, and its upper end was bolted to the lower end of the upper pipe segment. During installation, the verticality of the pipe was controlled by a crane, as shown in Fig. 5(d). This procedure was repeated until the designed depth of 25.6 m was reached. Fig. 5(e) shows a completed HDPE pile before filling, whereas Fig. 5(f) shows the backfilling of the pile with the sand-ceramsite mixture. Finally, the annular space between the pile-hole wall and the HDPE pipe was grouted with C15 concrete.

(a)



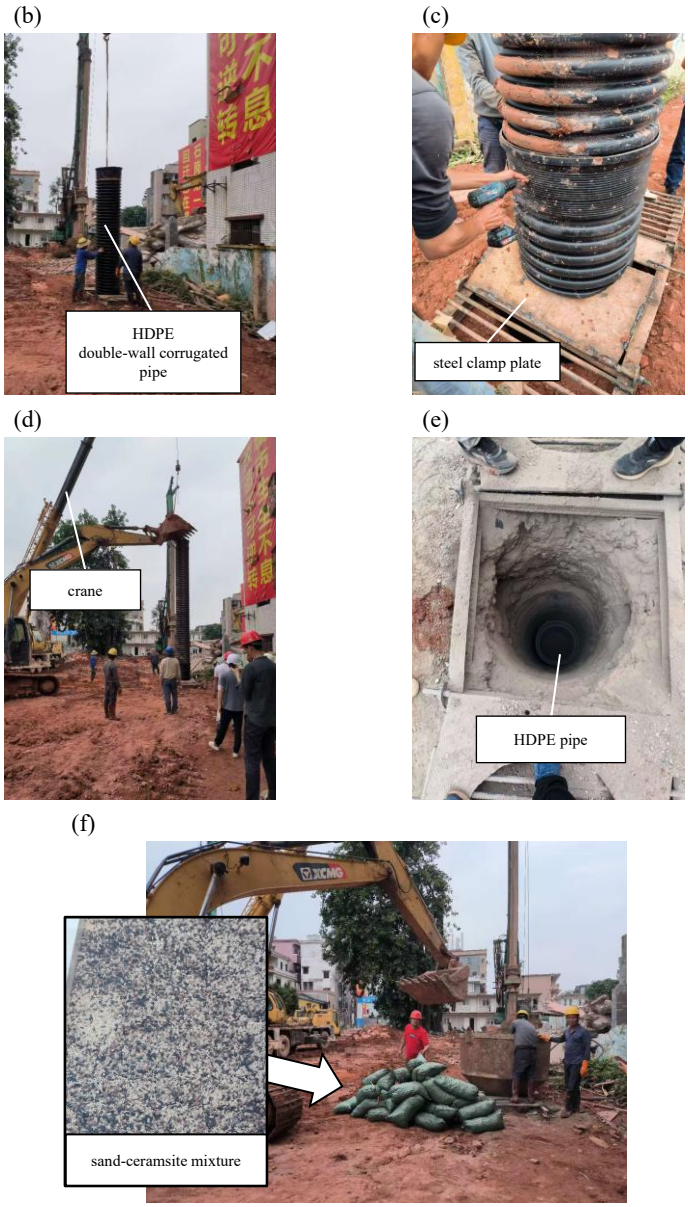


Fig. 5 Installation of the SCIPB: (a) installation procedure, (b) lifting and placement of an HDPE pipe, (c) connection and anchorage of HDPE pipe segments, (d) alignment and installation of the multi-segment HDPE pipe, (e) unfilled SCIPB, and (f) backfilling with the sand-ceramsite mixture.

2.4 Test setup for metro train-induced vibrations

Fig. 6 presents the test arrangement and data acquisition system used to measure metro train-induced vibrations. As shown in Fig. 6(a), three surface measurement points, denoted as A1, A2, and A3, were used to record vertical ground-surface accelerations induced by passing trains. These

points were located 8.5 m, 14.5 m, and 20.5 m from the SCIPB, respectively. In addition, receiver T1 was installed inside the tunnel and fixed to the tunnel wall at a height of 1.25 m above the rail, as shown in Fig. 6(b). A piezoelectric accelerometer with a sensitivity of 500 mV/(m/s²) was installed at each measurement point to record vertical acceleration signals. The ground-surface data were collected using a multi-channel data acquisition system connected to a laptop for data storage. The data acquisition system inside the tunnel was powered by batteries. Before each test, the two acquisition systems were synchronized, and the sampling frequency was set to 1000 Hz. The measurements were performed in two phases: (1) before installation of the SCIPB and (2) after construction of the SCIPB. In each phase, 20 sets of train-induced vibration data were synchronously recorded at all four measurement points.

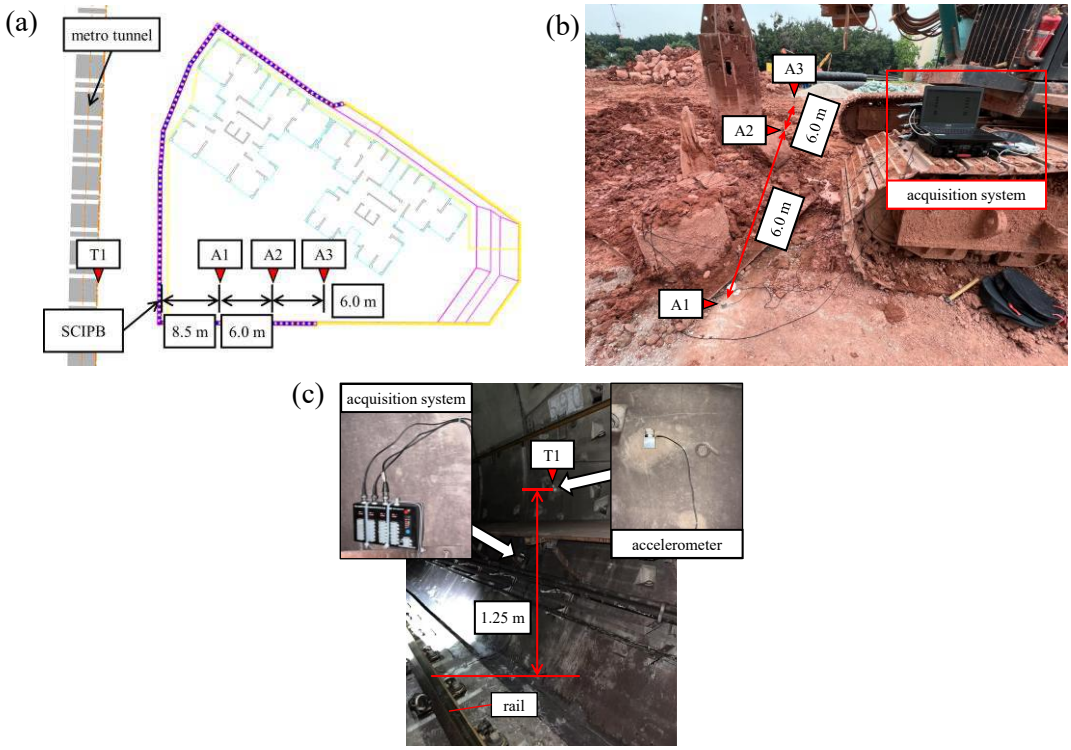


Fig. 6 In-situ test setup: (a) locations of the measurement points, (b) receivers A1, A2, and A3 on the ground surface, and (c) receiver T1 inside the tunnel.

2.5 Test results and discussion

Fig. 7 shows the time-history signal and frequency content of a typical metro train-induced vibration recorded at receiver T1 inside the tunnel. The signal clearly captures the arrival, passage, and departure of the train. The train passage lasted approximately 10 s, and the peak acceleration was 0.056 m/s². Within the frequency range of 0–100 Hz, the dominant vibration frequency was approximately 66 Hz.

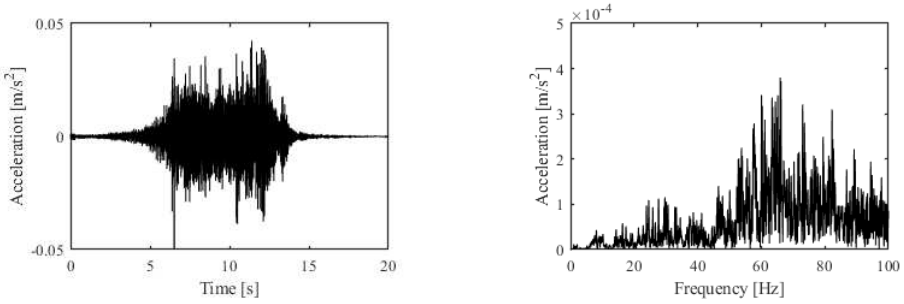
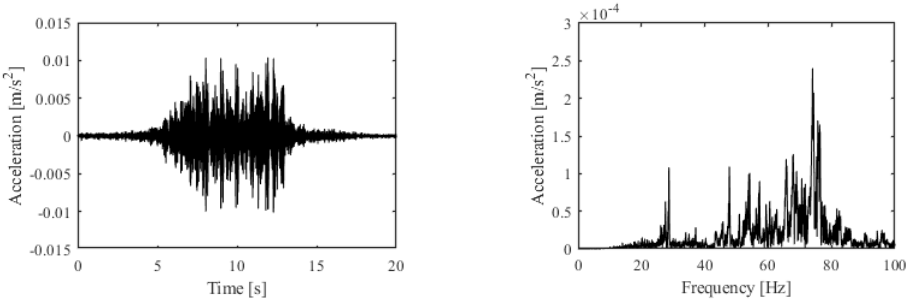


Fig. 7 Time history signal (left) and frequency content (right) of typical metro train-induced acceleration measured at receiver T1.

Fig. 8 presents the vertical ground-surface acceleration responses measured at A1–A3 before installation of the SCIPB. Compared with the peak acceleration measured at T1, the ground-surface vibrations were substantially attenuated as the waves propagated through the soil. The peak accelerations recorded at A1, A2, and A3 were 0.010 m/s², 0.007 m/s², and 0.008 m/s², respectively. This attenuation is mainly associated with the low-pass filtering effect of the soil (Degrande and Schillemans 2001). In the frequency domain, the dominant vibration components at the ground-surface measurement points were mainly within the range of 40–80 Hz. A second spectral peak was observed at approximately 26 Hz. This peak was attributed to resonance of the first two soil layers overlying the stiff underlying layer. The corresponding resonance frequency can be estimated as $\overline{C_{\mathrm{p}}} / 4d$ =24.24 Hz, where $\overline{C_{\mathrm{p}}}$ is the average dilatational-wave velocity of the upper two soil layers and d is their total thickness. The calculated result agrees well with the measured frequency.

(a)



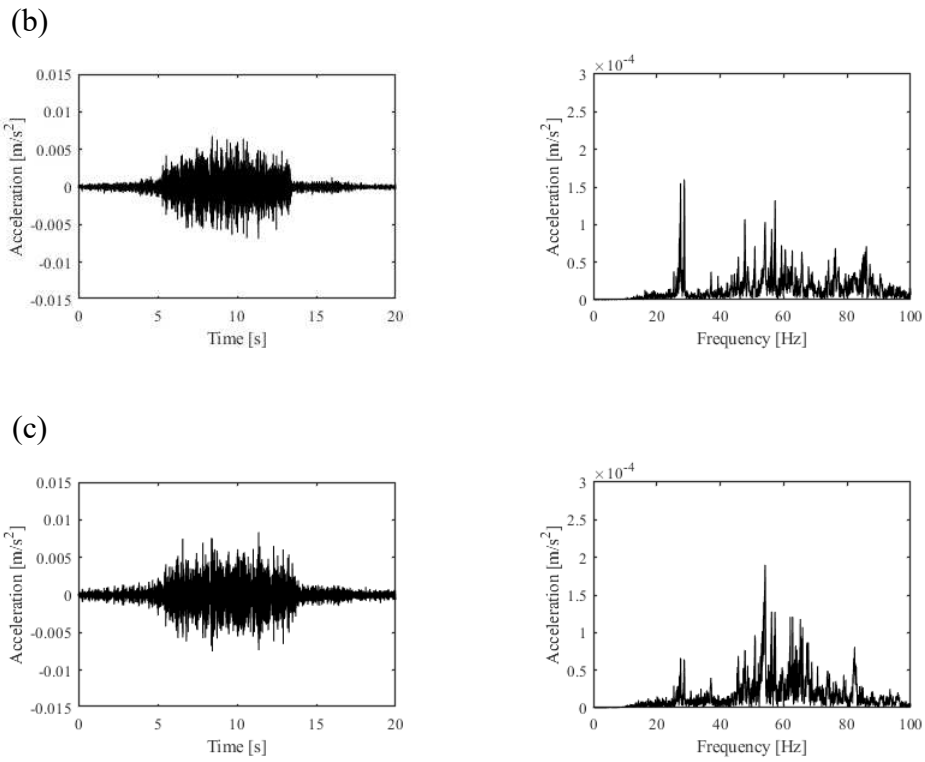
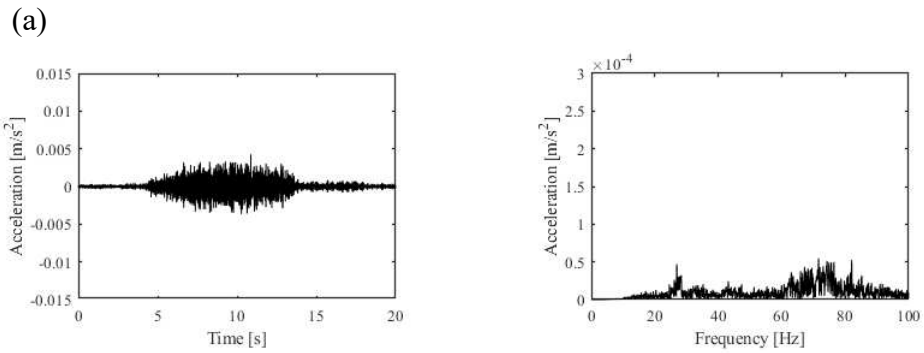


Fig. 8 Time history signals (left) and frequency content (right) of typical metro train-induced accelerations without the SCIPB at: (a) A1, (b) A2, and (c) A3.

As shown in Fig. 9, ground vibrations were significantly reduced after installation of the SCIPB, as indicated by both the time-history responses and frequency spectra. Compared with the results obtained without the SCIPB, the peak accelerations at A1, A2, and A3 decreased to 0.004 m/s², 0.003 m/s², and 0.004 m/s², respectively. These values correspond to reductions of approximately 59%, 63%, and 50%, respectively. In the frequency domain, the main vibration components were noticeably attenuated after installation of the SCIPB. However, the soil-resonance peak near 26 Hz remained evident.



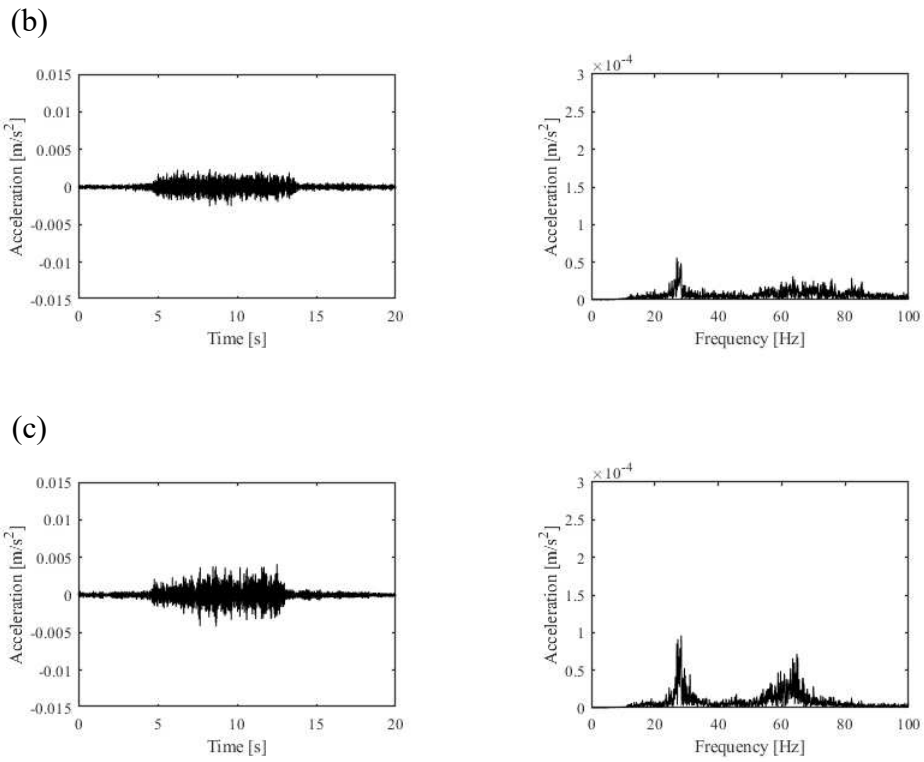


Fig. 9 Time history signals (left) and frequency content (right) of typical metro train-induced accelerations with SCIPB at: (a) A1, (b) A2, and (c) A3.

To further evaluate the vibration mitigation performance of the SCIPB, the average insertion loss ($\overline{IL}$) was calculated from the 20 measured data sets by comparing the acceleration spectra obtained with and without the SCIPB:

$$\overline{IL} = \sum_{j=1}^{m} 20\log_{10}\left(\left|\hat{a}_{z,j}^{w/o}\right| \Big/ \left|\hat{a}_{z,j}^{with}\right|\right) \tag{1}$$

where a hat symbol "$\hat{}$" denotes a variable in the frequency-spatial domain; $\hat{a}_{z,j}$ is the frequency-domain vertical acceleration for the *j*-th data set; the superscript "with" and "w/o" refer to the cases with and without the SCIPB, respectively; and *m* is the total number of data sets. A positive insertion loss indicates that the SCIPB reduces vertical vibrations.

As shown in Fig. 10, the insertion-loss curves are positive over most of the investigated frequency range at all measurement points, confirming the vibration mitigation effect of the SCIPB. The maximum reduction occurred at approximately 50 Hz, where the insertion losses at A1, A2, and A3 were 14.1 dB, 13.6 dB, and 14.6 dB, respectively. Above 50 Hz, the insertion loss generally decreased with increasing frequency. At 100 Hz, the insertion losses were 0.8 dB, 7.8 dB, and 10.7 dB at A1, A2, and A3, respectively. This trend indicates that the vibration reduction performance of the SCIPB for high-frequency components improved with increasing distance from the barrier. In contrast, below 10 Hz, the vibration mitigation effect gradually decreased from A1 to A3. This result suggests that the SCIPB was more effective in reducing low-frequency near-

field vibrations at locations closer to the vibration source. A clear vibration amplification was observed at A3 in the frequency range of 20–40 Hz, which was likely caused by soil resonance.

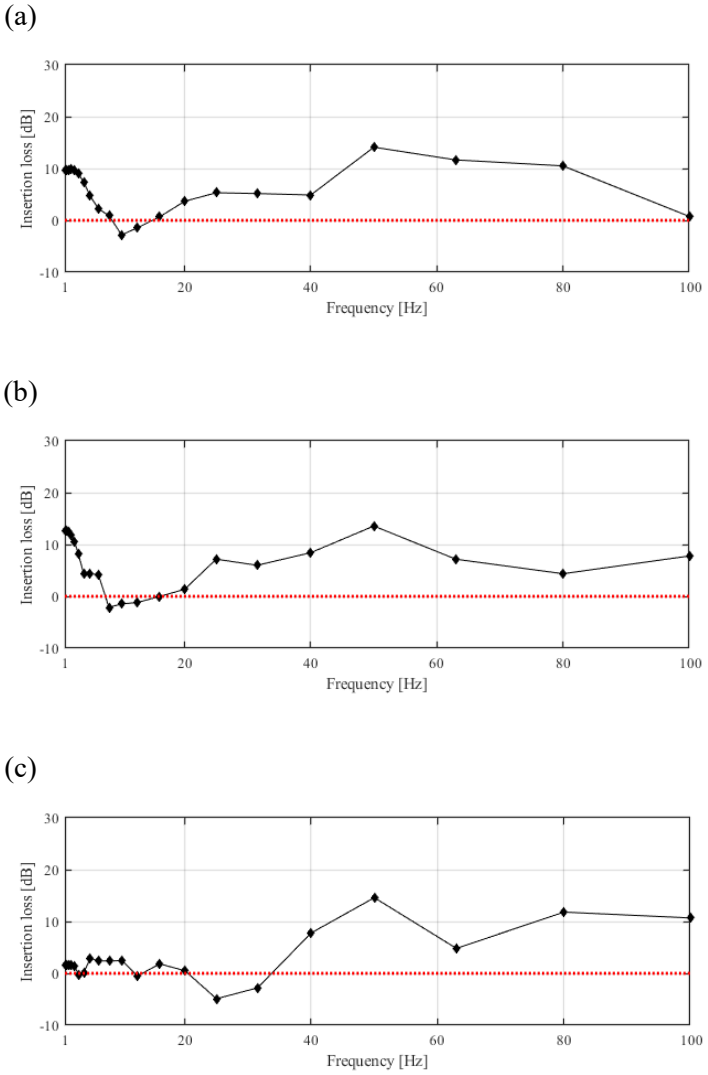


Fig. 10 Experimental average insertion loss of the SCIPB at: (a) A1, (b) A2, and (c) A3.

3. Numerical analysis

3.1 Finite element model of the SCIPB

Before conducting the parametric study, a three-dimensional tunnel-soil-SCIPB interaction model was developed in ANSYS to simulate metro train-induced ground vibrations. As shown in Fig. 11, the model is symmetric with respect to the *X*-*Z* plane. Therefore, only one half of the system was modeled to improve computational efficiency. The half-model has dimensions of 44

m×20 m×30 m. The model was discretized using SOLID185 elements. A global element size of 0.2 m was adopted, which is smaller than one-fifth of the minimum shear-wave wavelength in the site soil at the target frequency of 100 Hz (Xu et al. 2015). The final model contains approximately 1.2 million elements and 1.23 million nodes. The bottom boundary was fixed, whereas the ground surface was modeled as free. Normal-displacement constraints were imposed on the nodes located on the symmetry plane. A 2-m-thick three-dimensional perfectly matched layer (PML) was applied to all model boundaries except for the ground surface and the symmetry plane. The PML was used to absorb outgoing waves and minimize artificial wave reflections from the model boundaries. This feature was implemented by activating the PML option available in the SOLID185 element formulation. Under metro train-induced vibrations, all materials in the model were assumed to behave as linear elastic materials (Gupta et al. 2007; Chen et al. 2019). The sand-ceramsite mixture, with a sand-to-ceramsite volume ratio of 1:1, was modeled as a homogeneous material. Its properties were calculated as the average values of the properties of sand and ceramsite.

The responses at the three ground-surface receivers, A1–A3, were calculated using the frequency-domain transfer-function method, which has been validated by Luo and Deng (2024, 2025). This method involves two steps. First, the vertical vibration transfer function between the tunnel-wall receiver T1 and each ground-surface receiver was calculated numerically. Second, the vertical acceleration response at each ground-surface receiver was obtained by convolving the measured acceleration at T1 with the corresponding transfer function. This approach avoids the need to explicitly model the complex dynamic loads generated by moving trains.

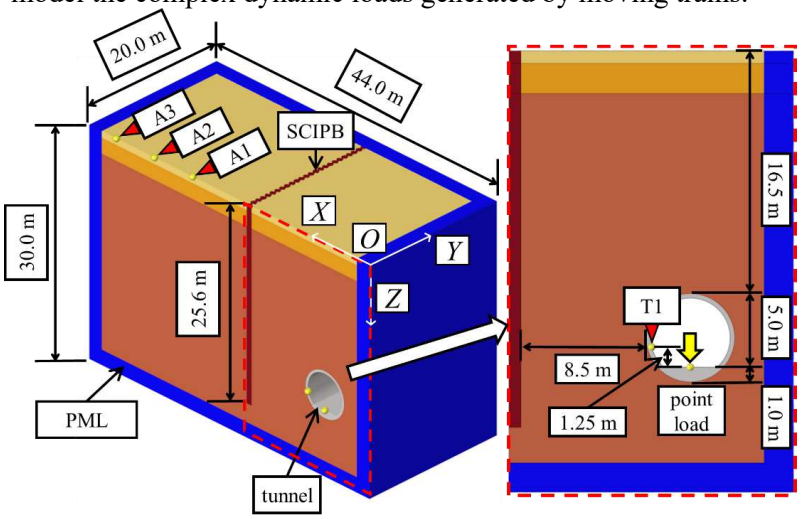


Fig. 11 Three-dimensional finite element model.

3.2 Comparison between experimental and numerical results

Figs. 12 and 13 compare the experimental and numerical vertical acceleration responses at A1–A3 for the cases without and with the SCIPB, respectively. The numerical time-history responses agree well with the measured results at all receiver locations, regardless of whether the SCIPB is installed. The differences between the numerical and experimental peak accelerations are generally within ±10%, which is considered acceptable for engineering analysis. In addition, the numerical results reproduce the main frequency components of the measured responses over the frequency

range of interest, up to 100 Hz.

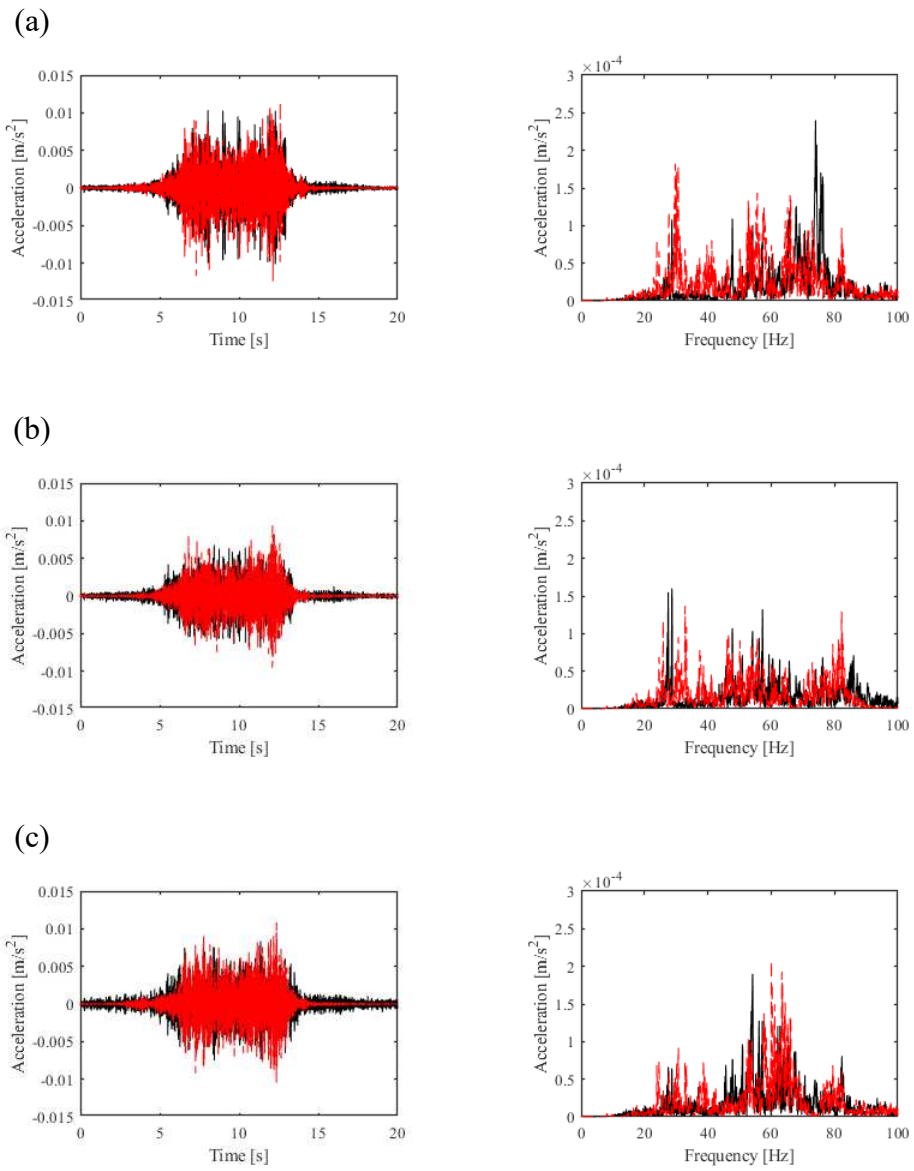


Fig. 12 Time history signals (left) and frequency content (right) of experimental (black solid line) and numerical (red solid line) metro train-induced accelerations without the SCIPB at: (a) A1, (b) A2, and (c) A3.

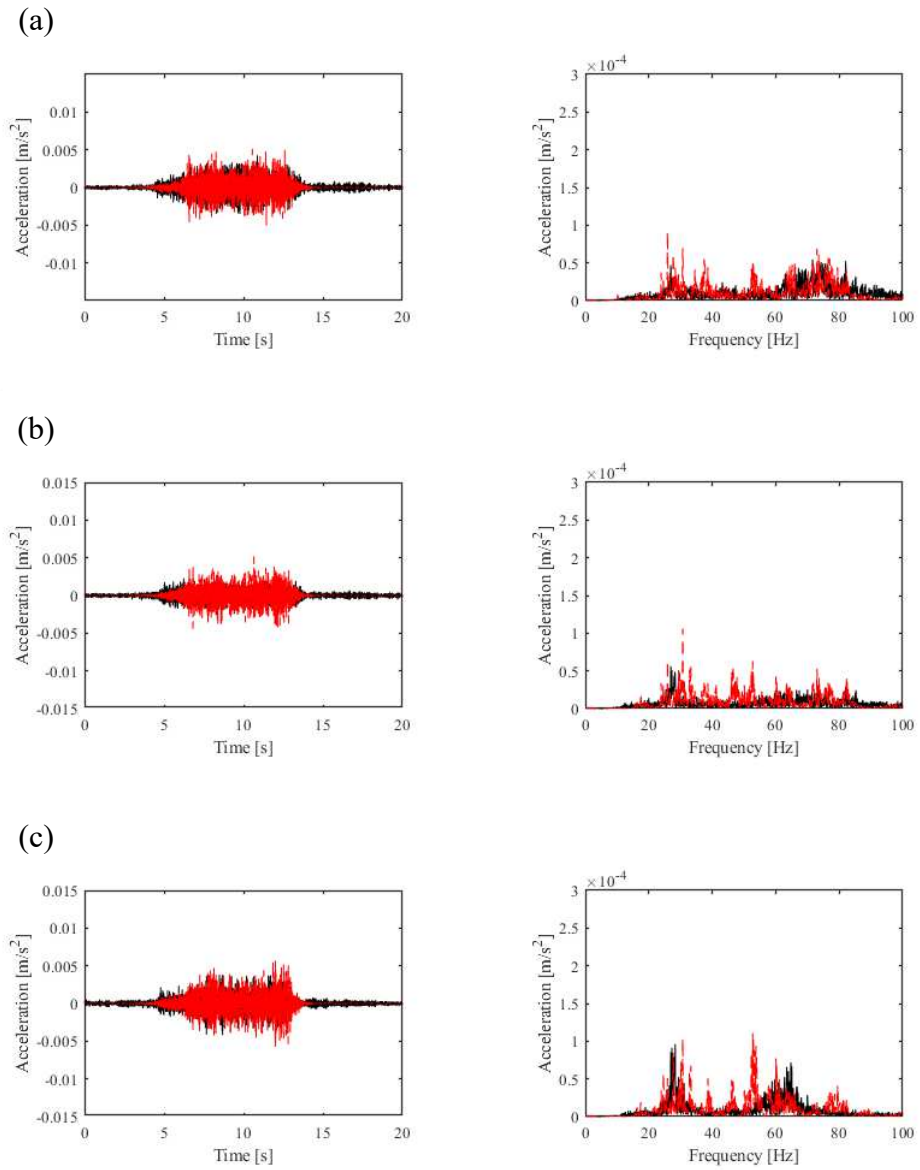


Fig. 13 Time history signals (left) and frequency content (right) of experimental (black solid line) and numerical (red solid line) metro train-induced accelerations with the SCIPB at: (a) A1, (b) A2, and (c) A3.

Fig. 14 compares the experimental and numerical average insertion losses at the three measurement points. The numerical results were obtained using the transfer-function method, with 20 sets of acceleration data measured at the tunnel-wall receiver T1 as input. As shown in the figure, the numerical and experimental curves exhibit similar overall trends and are in reasonable agreement. In particular, the numerical model captures the near-field vibration mitigation performance of the SCIPB well, with good agreement between the numerical and experimental results below 20 Hz. At higher frequencies, however, the numerical model generally slightly

underestimates the insertion loss. This difference may be attributed to the more complex wave propagation and radiation damping conditions at the test site than those represented in the idealized numerical model.

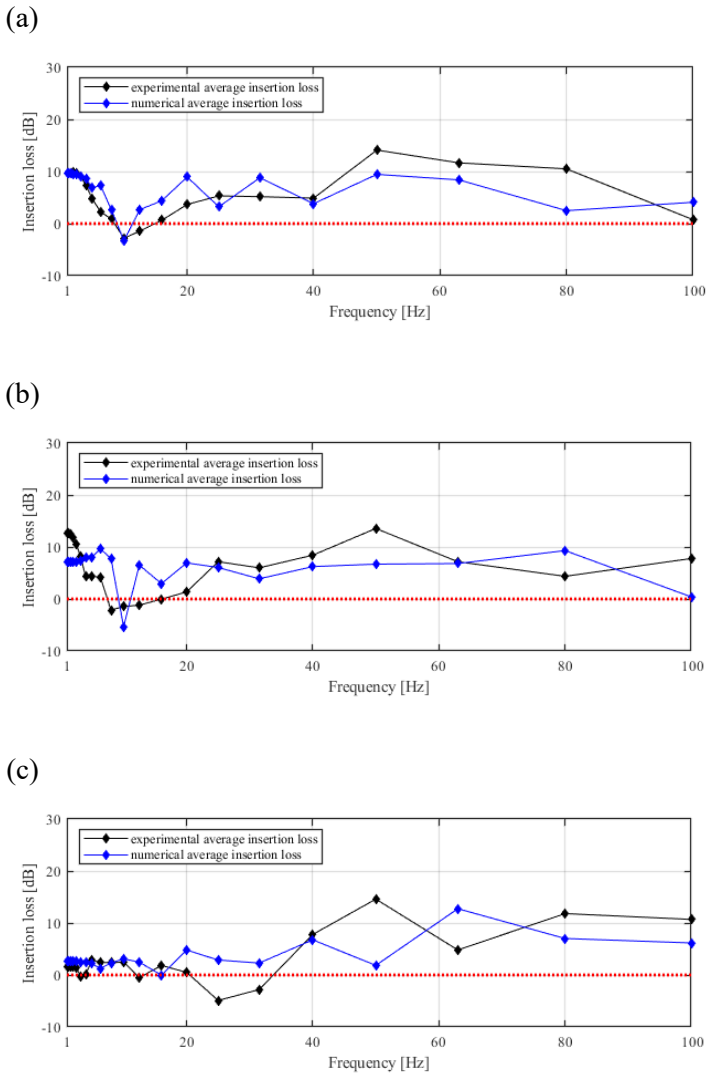


Fig. 14 Comparison of experimental (black solid line) and numerical (blue solid line) average insertion losses at: (a) A1, (b) A2, and (c) A3.

4. Parametric study

This section presents a parametric study of the SCIPB at the test site. The effects of three key parameters on vibration mitigation performance are investigated: the number of pile rows, the spacing between adjacent piles, and the in-fill material. As an example, Fig. 15 shows the cases with one, two, and three pile rows. The spacing between adjacent pile rows is fixed at 2.5 m,

which is commonly used in engineering practice. To evaluate the effects of these parameters comprehensively, the average insertion losses at A1–A3 are considered. In addition, an average amplitude reduction factor $\overline{AR_z}$ in the frequency domain is introduced following Woods (1968):

$$\overline{AR_z} = \frac{1}{A_{quadrant}} \int_{A_{quadrant}} AR_z d\Gamma \tag{2}$$

where $AR_z = \left| a_z^{with} \right| / \left| a_z^{w/o} \right|$ is the amplitude reduction factor, defined as the ratio of the vertical acceleration with the SCIPB to that without the SCIPB. $A_{quadrant}$ denotes a quarter-circular area behind the SCIPB with a radius of 18 m. An $\overline{AR_z}$ value below 1.0 indicates that the SCIPB reduces vertical vibrations.

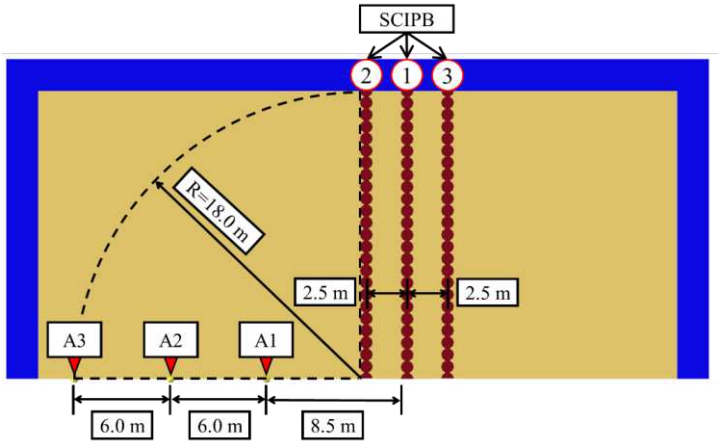


Fig. 15 Parametric study setup for evaluating the effect of the number of pile rows.

4.1 Effect of the number of pile rows

Fig. 16 presents the average insertion losses at A1–A3 and the average amplitude reduction factors for different numbers of pile rows. As shown in Figs. 16 (a), (b), and (c), the insertion loss generally increases as the number of pile rows increases. The triple-row SCIPB provides the best vibration mitigation performance at all three receivers. However, most of the improvement occurs when the barrier changes from one row to two rows, whereas the additional benefit of adding a third row is smaller. For example, at A1 and 50 Hz, the insertion losses of the single-, double-, and triple-row SCIPBs are 9.5 dB, 12.8 dB, and 15.3 dB, respectively. Thus, the insertion loss increases by 34.7% when the number of rows increases from one to two, but by only 19.5% when it increases from two to three. In addition, increasing the number of pile rows is more effective for far-field vibrations than for near-field vibrations. The maximum improvement in insertion loss is approximately 11 dB at A1 and 19 dB at A3. In Fig. 16 (d) further confirms the better overall performance of the triple-row SCIPB. As shown in Fig. 17, increasing the number of pile rows reduces vibration amplification in the area behind the barrier. At the same time, stronger wave reflections can be observed in front of the SCIPB. However, when the evaluation area is extended from a single measurement point to the entire quarter-circular area, the double-row and triple-row SCIPBs show similar performance above 60 Hz. Therefore, at this test site, simply adding more pile rows may not provide a significant additional benefit for mitigating high-frequency vibrations.

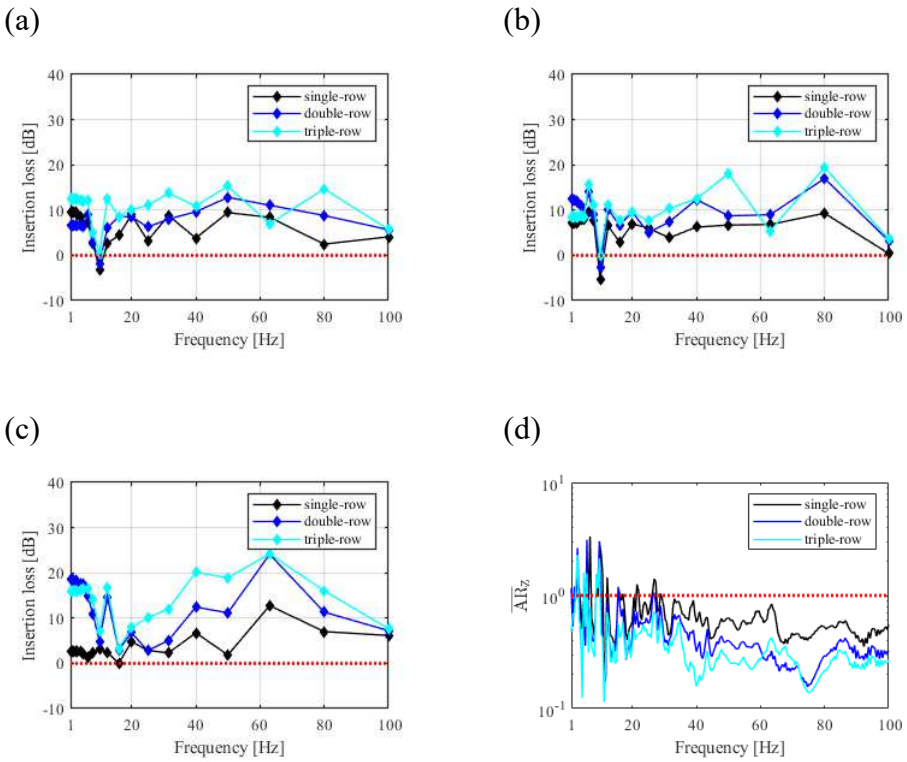


Fig. 16 Average insertion loss at (a) A1, (b) A2, and (c) A3, and (d) average amplitude reduction factor versus loading frequency for different numbers of pile rows.

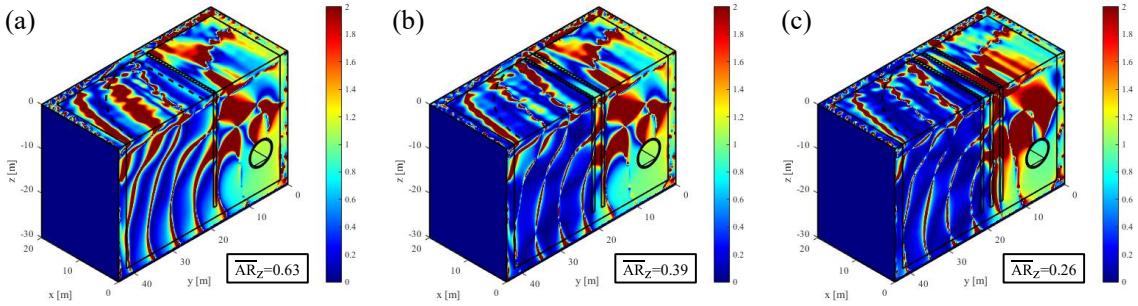


Fig. 17 Contour maps of the amplitude reduction factor induced by a unit point load at 50 Hz for different numbers of pile rows: (a) single-row SCIPB, (b) double-row SCIPB, and (c) triple-row SCIPB.

4.2 Effect of the spacing between adjacent piles

In addition to the number of pile rows, the spacing between adjacent piles is an important factor affecting both construction cost and vibration mitigation performance. The reference case has a pile spacing of 1D (0.8 m), where D is the pile diameter. Two additional cases are considered: a spacing of 2D (1.6 m) and a zero-spacing case. The latter represents a continuous in-filled trench with a uniform cross-section along the *Y*-direction.

Fig. 18 shows the average insertion losses at A1–A3 and the average amplitude reduction factors for different pile spacings. As shown in Figs. 18 (a), (b), and (c), the insertion loss increases as the pile spacing decreases. The continuous in-filled trench provides the best vibration mitigation performance at all three receivers because it creates the largest stiffness contrast along the wave propagation path. Notably, the insertion losses of the 1D-spacing case reach approximately 90% of those of the continuous in-filled trench over most of the frequency range of interest. This result indicates that the SCIPB can provide vibration mitigation performance close to that of an in-filled trench while requiring less sand-ceramsite material. In contrast, when the pile spacing increases from 1D to 2D, the vibration reduction effect almost disappears. In Fig. 18 (d), the average amplitude reduction factors further confirm that the 2D pile spacing case exhibits nearly no vibration reduction. As illustrated in Fig. 19 (c), waves can diffract through the gaps between adjacent piles when the spacing is large. Therefore, the spacing between piles should be carefully controlled. Adjacent piles should preferably be tangent or interlocked to ensure effective vibration isolation.

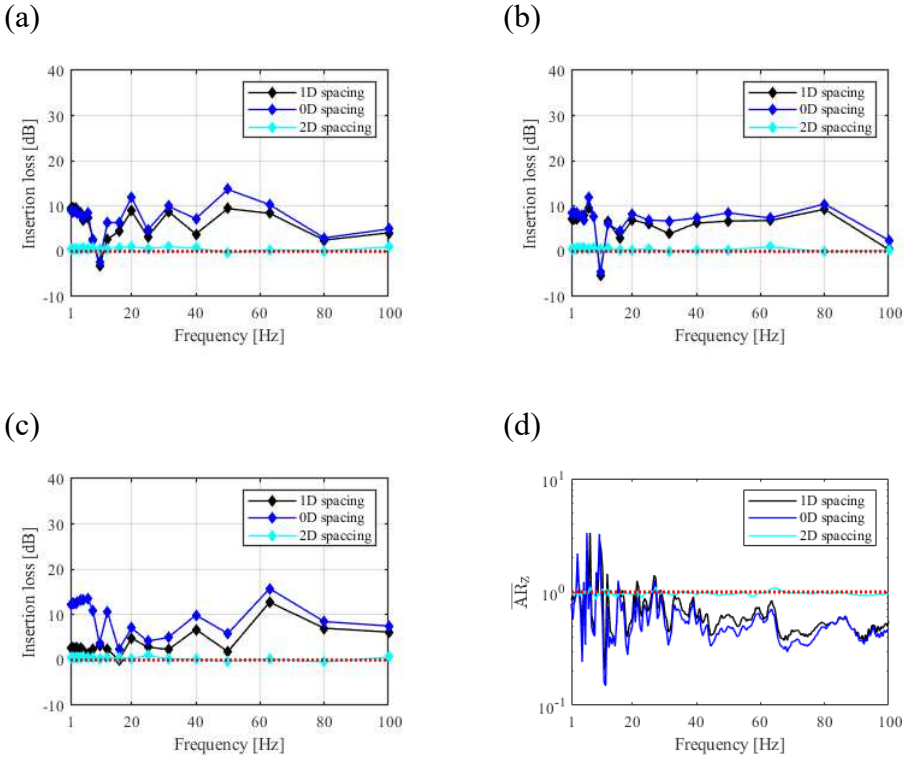


Fig. 18 Average insertion loss at (a) A1, (b) A2, and (c) A3, and (d) average amplitude reduction factor versus loading frequency for different pile spacings.

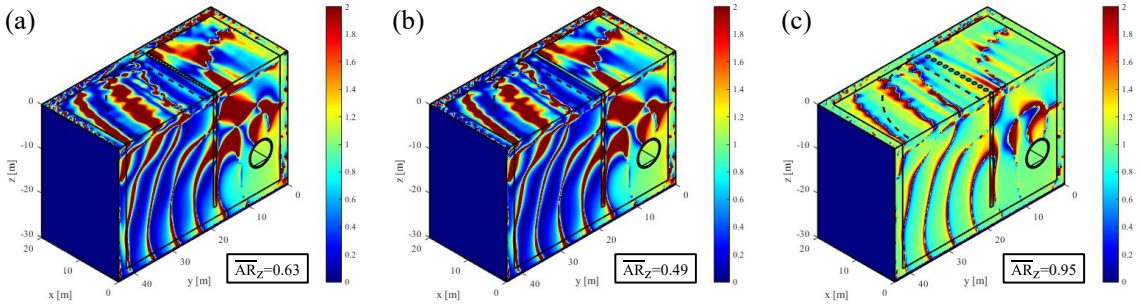


Fig. 19 Contour maps of the amplitude reduction factor induced by a unit point load at 50 Hz for different pile spacings: (a) pile spacing of 1D, (b) pile spacing of 0D (i.e., continuous in-filled trench), and (c) pile spacing of 2D.

4.3 Effect of the pile's in-filled materials

As described in Section 2.1, the sand-ceramsite mixture was designed to provide a suitable particle-size distribution, minimize large voids, and maintain sufficient density to resist buoyancy during construction. However, sand and ceramsite have substantially different material properties. For example, the Young's modulus of sand is nearly ten times that of ceramsite. Therefore, the effect of the mixing ratio on the vibration mitigation performance of the SCIPB should be examined. Two limiting cases were considered in addition to the sand-ceramsite mixture: piles filled entirely with sand and piles filled entirely with ceramsite.

Fig. 20 shows the average insertion losses at A1–A3 and the average amplitude reduction factors for the three in-fill materials. As shown in Figs. 20 (a), (b), and (c), the insertion loss generally increases as the Young's modulus of the in-fill material decreases. The ceramsite-filled case provides the best vibration mitigation performance at all three receivers, whereas the sand-filled case performs the worst over most of the frequency range of interest. The performance of the sand-ceramsite SCIPB lies between these two limiting cases. The main differences among the three cases occur in the frequency range of 1–80 Hz. At frequencies above 80 Hz, their vibration mitigation performance becomes similar. This is because the wavelengths of the propagating waves become much shorter at high frequencies, reducing the influence of the differences in in-fill material properties. Fig. 20 (d) and Fig. 21 further show that vibration mitigation improves as the stiffness contrast between the surrounding soil and the in-fill material increases. Therefore, provided that adequate resistance to buoyancy is maintained during construction, increasing the proportion of ceramsite can improve the vibration mitigation performance of the SCIPB, particularly below 80 Hz.

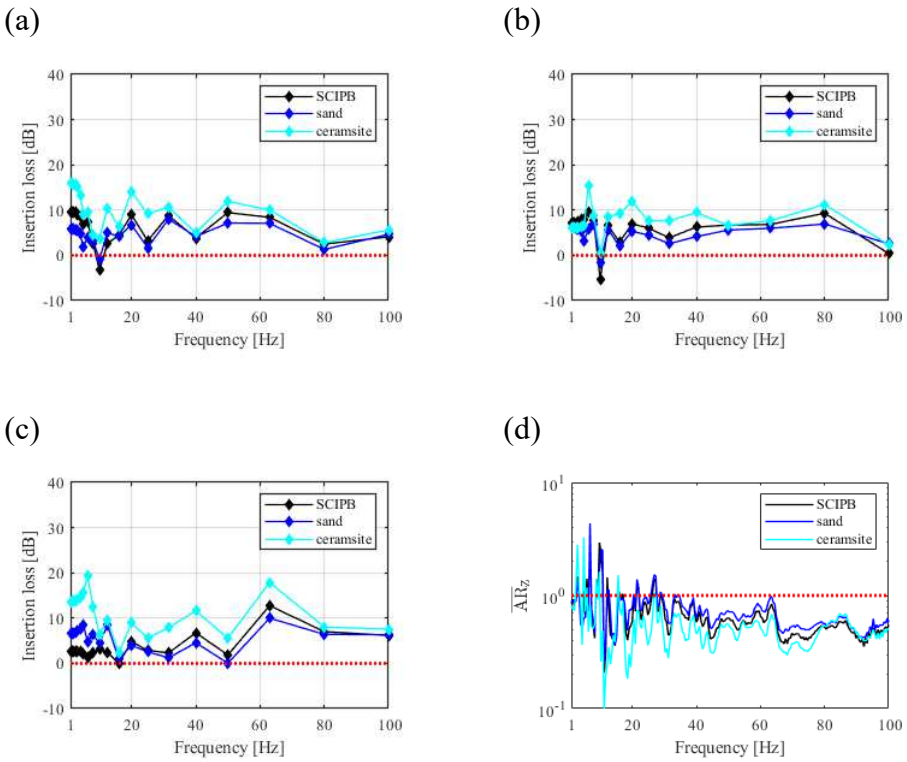


Fig. 20 Average insertion loss at (a) A1, (b) A2, and (c) A3, and (d) average amplitude reduction factor versus loading frequency for different in-filled materials.

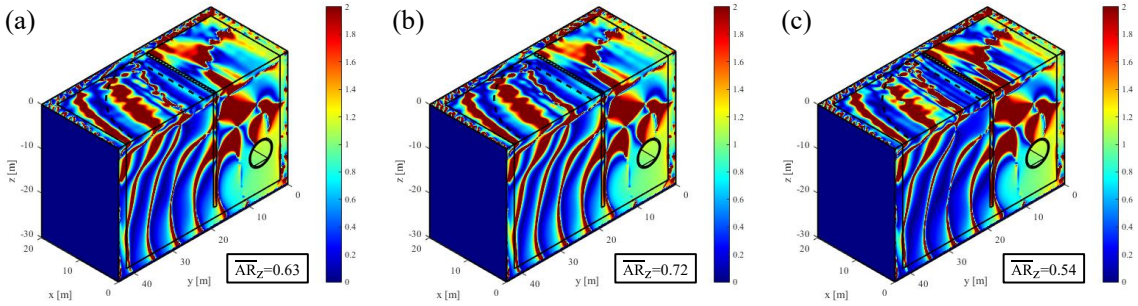


Fig. 21 Contour maps of the amplitude reduction factor induced by a unit point load at 50 Hz for different in-filled materials: (a) sand-ceramsite mixture, (b) sand, and (c) ceramsite

5. Conclusions

This study proposed and applied a sand–ceramsite in-filled pile barrier (SCIPB) to mitigate metro train-induced vibrations. The field application of the SCIPB was described in detail, and its vibration mitigation performance was evaluated through in-situ measurements. After validation against the field results, a numerical model was used to investigate the effects of the number of pile rows, pile spacing, and in-fill material on vibration mitigation performance. The main

conclusions are as follows:

(a) The in-situ test results show that the SCIPB reduced the peak accelerations of metro train-induced vibrations by approximately 50–63%. The maximum average insertion losses ranged from 13.6 to 14.6 dB.

(b) The vibration mitigation performance of the SCIPB generally improves as the number of pile rows increases. However, when more than two rows are used, the additional improvement is limited at frequencies above 60 Hz.

(c) Pile spacing has a strong influence on the effectiveness of the SCIPB. Adjacent piles should be tangent or interlocked to provide effective vibration isolation. Large gaps between piles allow wave diffraction and can substantially reduce the mitigation effect.

(d) The vibration mitigation performance of the sand-ceramsite SCIPB lies between that of sand-filled and ceramsite-filled pile barriers. Using an in-fill material with a lower Young's modulus can improve the performance of the SCIPB, especially at frequencies below 80 Hz.

Overall, the field measurements and numerical analyses confirm that the SCIPB is an effective measure for mitigating metro train-induced vibrations. The parametric results also provide useful guidance for the practical design of SCIPBs. However, the present findings are based on the soil conditions at the test site. Site-specific analysis and careful design are therefore necessary before applying the SCIPB in other projects.

References

Ai, Z.Y., Cao, Z.: Vibration isolation of row of piles embedded in transverse isotropic multi layered soils. Comput. Geotech. **99**, 115–129 (2018). https://doi.org/10.1016/j.compgeo.2018.03.002

Alsharo, A., Douier, K., Hussein, M.F.M., et al.: Investigating the effect of using softer rail-pads on ground-borne vibration from underground railways. Int. J. Rail Transp. **12**(5), 803–826 (2024). https://doi.org/10.1080/23248378.2023.2256735

Bhattacharjee, N., Sur, A., Manna, B., Banerjee, A., Shahu, J.T.: ANN-Based Approach for the Prediction of Peak Particle Velocity of Ground Induced by Underground Metro Operations. Transp. Infrastruct. Geotechnol. **12**, 96 (2025). https://doi.org/10.1007/s40515-025-00541-8

Cao, X., Zhou, F., Liu, J., Ma, Q.: Experimental study and numerical analysis for vibration isolation performance on open trench and wave impeding block combined vibration isolation barrier. Soil Dyn. Earthq. Eng. **177**, 108418 (2024). https://doi.org/10.1016/j.soildyn.2023.108418

Celebi, E., Kirtel, O., Istegun, B., et al.: High-speed train induced environmental vibrations: Experimental study on isolation efficiency of recyclable in-filling materials for thin-walled hollow wave barrier. Eng. Struct. **312**, 118207 (2024). https://doi.org/10.1016/j.engstruct.2024.118207

Chango, I.V.L., Chen, J., Han, Z., Du, H.: Evaluating Vibration Control Barriers' Efficiency Near Maglev Train Viaduct: A Numerical and Statistical Approach. Transp. Infrastruct. Geotechnol. **12**, 98 (2025). https://doi.org/10.1007/s40515-024-00493-5

Chen, J., Zhuang, Y., Fang, H., et al.: Energy absorption of foam-filled lattice composite cylinders under lateral compressive loading. Steel Compos. Struct. **31**(2), 133–148 (2019). https://doi.org/10.12989/scs.2019.31.2.133

Chew, J.H., Leong, E.C.: Field and numerical modelling of sand-rubber mixtures vibration barrier. Soil Dyn. Earthq. Eng. **125**, 105740 (2019). https://doi.org/10.1016/j.soildyn.2019.105740

Dai, C.Q., Xin, T., Wang, S., et al.: Vibration source characteristics and vibration reduction mechanism of the novel rubber pad floating slab track in metro turnout areas. Eng. Struct. **332**, 120107 (2025). https://doi.org/10.1016/j.engstruct.2025.120107

Degrande, G., Schillemans, L.: Free field vibrations during the passage of a Thalys high-speed train at variable speed. J. Sound Vib. **247**(1), 131–144 (2001). https://doi.org/10.1006/jsvi.2001.3718

Dijckmans, A., Coulier, P., Jiang, J., et al.: Mitigation of railway induced ground vibration by heavy masses next to the track. Soil Dyn. Earthq. Eng. **75**, 158–170 (2015). https://doi.org/10.1016/j.soildyn.2015.04.003

Ding, G., Bao, J., Liu, Y.: Blocking effect of double-row periodic pile barriers with honeycomb-pored structure on vibration isolation. J. Vib. Control **32**(13–14), 4026–4039 (2026). https://doi.org/10.1177/10775463251347369

Fiala, P., Degrande, G., Augusztinovicz, F.: Numerical modelling of ground-borne noise and vibration in buildings due to surface rail traffic. J. Sound Vib. **301**(3–5), 718–738 (2007). https://doi.org/10.1016/j.jsv.2006.10.019

Gao, X., Yi, Q., Lei, J.X., et al.: Experimental study on the characteristics of vibration energy propagation in the subway turnout area. Constr. Build. Mater. **409**, 134210 (2023). https://doi.org/10.1016/j.conbuildmat.2023.134210

Gupta, S., Hussein, M.F.M., Degrande, G., et al.: A comparison of two numerical models for the prediction of vibrations from underground railway traffic. Soil Dyn. Earthq. Eng. **27**(7), 608–624 (2007). https://doi.org/10.1016/j.soildyn.2006.12.007

Jauhari, N., Chakrabortty, P., Hegde, A.: Numerical Investigation to Mitigate Train-Induced Ground Vibrations Using Dual Open or Geofoam-Infilled Barriers. Transp. Infrastruct. Geotechnol. **13**, 191 (2026). https://doi.org/10.1007/s40515-026-00961-0

Jazebi, M., Ahmadi, M.M., Sahebalzamani, P.: Efficiency of in-filled (geofoam) trenches in mitigating train-induced vibrations: A case study of Tehran-Tabriz railway. Constr. Build. Mater. **309**, 125075 (2021). https://doi.org/10.1016/j.conbuildmat.2021.125075

Kavand, A., Khadangi, A.: Field testing on active isolation of vibrating foundations in middle-frequency range. Constr. Build. Mater. **374**, 130893 (2023). https://doi.org/10.1016/j.conbuildmat.2023.130893

Kumar, S., Jauhari, N., Kumar, R., Chakrabortty, P.: Experimental Approach to Ground Vibration Mitigation using Dual Barriers-Filled with Different Materials. Transp. Infrastruct. Geotechnol. **13**, 75 (2026). https://doi.org/10.1007/s40515-026-00848-0

Li, S.Y.: Analysis of the vibration mitigation effects of pile barrier in unsaturated ground using the coupled BE and FE method. Eng. Anal. Bound. Elem. **162**, 284–309 (2024). https://doi.org/10.1016/j.enganabound.2024.02.006

Liu, X., Bai, W., Dai, J., et al.: Optimization of TMDs for floor vibration control in metro-adjacent buildings considering frequency weighting. J. Vib. Control (2026). https://doi.org/10.1177/10775463261475998

Luo, W.L., Deng, S.B.: A rubber-coated bored pile in isolating metro-induced vibrations: Concept, analytical and in-situ investigation. Constr. Build. Mater. **426**, 136094 (2024). https://doi.org/10.1016/j.conbuildmat.2024.136094

Luo, W.L., Deng, S.B.: Numerical and in-situ investigation on bilateral double-wall barriers in mitigating metro train-induced vibrations. Constr. Build. Mater. **469**, 140502 (2025). https://doi.org/10.1016/j.conbuildmat.2025.140502

Luo, W.L., Deng, S.B.: Field application of polyurethane foam in-filled pile barrier in mitigating metro train-induced building vibrations. Int. J. Struct. Stab. Dyn. 2750106 (2026a). https://doi.org/10.1142/S0219455427501069

Luo, W.L., Deng, S.B.: Mitigation of metro train-induced over-track super high-rise building vibrations using laminated rubber bearings: Field application. Structures **85**, 111167 (2026b). https://doi.org/10.1016/j.istruc.2026.111167

Luo, W.L., Liang, Q.H., Zhou, Y., et al.: A novel three-dimensional isolation bearing for buildings subject to metro- and earthquake-induced vibrations: Laboratory test and application. J. Build. Eng. **86**, 108798 (2024). https://doi.org/10.1016/j.jobe.2024.108798

Luo, W.L., Yin, Y.J.: A novel wave barrier incorporating local resonators for mitigating metro-induced vibrations. Eng. Struct. **351**, 122048 (2026). https://doi.org/10.1016/j.engstruct.2025.122048

Luo, W.L., Yin, Y.J., Deng, S.B., et al.: A novel periodic in-filled metabarrier for mitigating train-induced vibrations. Soil Dyn. Earthq. Eng. **206**, 110252 (2026). https://doi.org/10.1016/j.soildyn.2026.110252

Moussa, A., El Naggar, H., Zhang, M.: Using tire derived aggregates (TDA) as infill material for wave

barriers. Soil Dyn. Earthq. Eng. **185**, 108866 (2024). https://doi.org/10.1016/j.soildyn.2024.108866
Ni, Y., Wu, L., Cheng, Z., Shi, Z.: Vibration mitigation of a transit-oriented development building based on periodic theory. Soil Dyn. Earthq. Eng. **190**, 109202 (2025). https://doi.org/10.1016/j.soildyn.2024.109202
Pu, Q., Wei, K., Liu, Y., Wang, X., Li, J.: Design method of track dynamic stiffness based on Z-vibration level insertion loss evaluation and field measurement verification. Constr. Build. Mater. **472**, 140917 (2025). https://doi.org/10.1016/j.conbuildmat.2025.140917
Ren, Y., Qu, S., Yang, J., Li, Q., Zhu, B., Zhai, W., et al.: An efficient three-dimensional dynamic stiffness-based model for predicting subway train-induced building vibrations. J. Build. Eng. **76**, 107239 (2023). https://doi.org/10.1016/j.jobe.2023.107239
Shan, Y., Cheng, G.H., Gu, X.Q., et al.: Optimization of design parameters of displacement isolation piles constructed between a high-speed railway bridge and a double-line metro tunnel: From the view point of vibration isolation effect. Comput. Geotech. **140**, 104460 (2021). https://doi.org/10.1016/j.compgeo.2021.104460
Surapreddi, S., Ghosh, P.: Active vibration screening characteristics of bamboo in-filled wave barriers. Soil Dyn. Earthq. Eng. **171**, 107945 (2023). https://doi.org/10.1016/j.soildyn.2023.107945
Wang, H.Z., Zhang, C.S., Jiang, J.Q., et al.: Vibration characteristics and isolation in vibration-sensitive areas under moving vehicle load. Soil Dyn. Earthq. Eng. **153**, 107077 (2022). https://doi.org/10.1016/j.soildyn.2021.107077
Woods, R.D.: Screening of surface wave in soils. J. Soil Mech. Found. Div. **94**(4), 951–979 (1968). https://doi.org/10.1061/JSFEAQ.0001180
Xiao, P., Miao, L., Zheng, H., et al.: Novel phononic-like crystal pile structure with low-frequency and multi-frequency band gaps for vibration isolation. J. Vib. Control **32**(11–12), 3281–3297 (2026). https://doi.org/10.1177/10775463251344367
Xu, Q.Y., Xiao, Z.C., Liu, T., et al.: Comparison of 2D and 3D prediction models for environmental vibration induced by underground railway with two types of tracks. Comput. Geotech. **68**, 169–183 (2015). https://doi.org/10.1016/j.compgeo.2015.04.011
Yang, S., Jia, M.C.: A 3D coupled ALEM-BEM method for assessing pile mitigation performance to moving-harmonic-load induced vibrations in cross-anisotropic porous saturated media. Comput. Geotech. **163**, 105725 (2023). https://doi.org/10.1016/j.compgeo.2023.105725
Zhang, X., Luo, W.L., Lin, B.H., et al.: Vibration isolation effects of barriers filled with ceramsite and sand: Full-scale model test and numerical investigation. Constr. Build. Mater. **341**, 127789 (2022). https://doi.org/10.1016/j.conbuildmat.2022.127789
Zou, C., Zhao, Y., Luo, W., Guo, W., Shen, Z.: Dynamic coupling mechanisms and hybrid mitigation of vibration transmission in metro depot climbing lines. Constr. Build. Mater. **492**, 142873 (2025). https://doi.org/10.1016/j.conbuildmat.2025.142873